Chuangnan Su, Deshun Liu, Siwen Tang*, Pengnan Li and Xinyi Qiu

Finite Element Analysis of Surface Residual Stress in Functionally Gradient Cemented Carbide Tool

DOI 10.1515/htmp-2016-0085
Received April 27, 2016; accepted January 26, 2017

Abstract: A component distribution model is proposed for three-component functionally gradient cemented carbide (FGCC) based on electron probe microanalysis results obtained for gradient layer thickness, microstructure, and elemental distribution. The residual surface stress of FGCC-T5 tools occurring during the fabrication process is analyzed using an ANSYS-implemented finite element method (FEM) and X-ray diffraction. A comparison of the experimental and calculated values verifies the feasibility of using FEM to analyze the residual surface stress in FGCC-T5 tools. The effects of the distribution index, geometrical shape, substrate thickness, gradient layer thickness, and position of the cobalt-rich layer on residual surface stress are studied in detail.

Keywords: functionally gradient cemented carbide, surface residual stress, finite element method

PACS® (2010). 81.05.Mh, 02.70.Dh

Introduction

As the manufacturing industry has rapidly developed, the complex coupling between the thermal and mechanical properties of the tool–chip region in the cutting process has reduced the life expectancy of the tools [1]. Thus, it is necessary to develop new tools to reduce costs and improve machining efficiency, quality, and accuracy. In recent years, functionally gradient cemented carbides (FGCCs) have been widely used in the cutting tool field [2]. The component and structural design of FGCCs not only solves the contradiction between hardness and toughness of a homogeneous material, but also enhances the bonding strength by reducing the thermal mismatch between the gradient layer and substrate [3]. Therefore, the use of FGCC cutting tools is an effective way of improving cutting performance.

FGCCs are mainly prepared using the construction and element-diffusion methods [4]. Samples made using the construction method are vulnerable to cracking or deformation due to the sudden changes in sintering shrinkage between the layers. However, FGCC tool prepared using the diffusion method possesses a chemical gradient that is continuous [5]. Furthermore, this gradient can be controlled to meet application requirements by optimizing the sintering process and alloy composition. Microwave sintering has been used in the FGCC fabrication process in recent years due to the advantages of volumetric, rapid and selective heating [6].

Breval [7] prepared WC–Co using microwave sintering, claiming that the process used had improved performance with regard to shrinkage uniformity, hardness, and anti-corrosion/erosion properties (compared to conventionally sintered samples). According to Lin [8], WC–Co FGCC prepared via microwave sintering has crystal particles that are smaller and have better mechanical properties due to the lower activation energy of the WC and selective heating attributed to the microwave processing. Tang [9] proposed a microwave-assisted nitriding–sintering method for preparing TiCN–Co–WC FGCC. By using a combination of the sintering and nitriding processes, high energy efficiency and rapid fabrication of the FGCC was thereby achieved.

High residual thermal stress is formed in the gradient layers because of the marked variation in thermal expansion from the surface of a sample to its center [10]. The mechanical properties and life expectancy of a cutting tool, however, can be improved by having residual compressive stress on the tool's surface [11, 12]. The thermal and mechanical problems presented by FGCCs are very complicated because the gradient layers are heterogeneous both microscopically and macroscopically. Fortunately, the finite element method (FEM) has proved to be an effective means of calculating the residual thermal stress. Williamson [13, 14] studied the residual stress associated with the

***Corresponding author: Siwen Tang,** Hunan Provincial Key Laboratory of Health Maintenance for Mechanical Equipment, Hunan University of Science and Technology, Xiangtan 411201, China, E-mail: siw_tang@hnust.edu.cn
Chuangnan Su, Deshun Liu, Hunan Provincial Key Laboratory of Health Maintenance for Mechanical Equipment, Hunan University of Science and Technology, Xiangtan 411201, China
Pengnan Li, Xinyi Qiu, Hunan Provincial Key Laboratory of High Efficiency and Precision Machining of Difficult-to-Cut Material, Hunan University of Science and Technology, Xiangtan 411201, China

gradient interface between a ceramic and metal during the cooling process by making use of elastic–plastic FEM. It was found that the residual stress was strongly influenced by the geometry of the materials. Huang [15] analyzed the distribution of the residual thermal stress in WC-6Co samples using FEM and X-ray diffraction (XRD) measurements. It was shown that compressive and tensile stresses were formed in the surface and cobalt-rich zones, respectively.

A power-function component distribution model is usually employed to describe the residual stress of FGCCs because it is more convenient to use with the distribution index n [16]. Ai [17] designed an Al_2O_3/TiC graded ceramic to create residual compressive stress in surface layers. This work showed that the best tool performance can be achieved when the thermal expansion coefficient of the surface layer is lower than that of all the inner layers. Xu [18] prepared Al_2O_3/TiC/CaF_2 gradient self-lubricating ceramic tools based on a proposed multi-component distribution model with microstructures consistent with a component distribution function.

Previous research has focused on analyzing the residual stress of FGCCs containing no more than two components [19]. For this paper, FGCC cutting tools (FGCC-T5) were prepared using microwave-assisted nitriding sintering. The resulting microstructures and element distributions were analyzed using electron probe microanalysis (EPMA). A three-component gradient distribution function for the FGCC-T5 tools is proposed and the residual stress created in the fabricating process is analyzed. The effect of varying different gradient layer parameters on the residual stress of the FGCC-T5 is further studied using a combination of FEM and experimental work.

Gradient component distribution characteristics

Gradient structure and elemental distribution of the FGCC-T5 tools

The original materials chosen to use are WC, TiC, and cobalt (with proportions amounting to 85 %, 5 %, and 10 %, respectively). The FGCC-T5 cutting tools were prepared using the previously-described microwave-assisted nitriding sintering method [9, 20, 21]. After production, cross-sectional metallographic specimens were prepared. The gradient structure and elemental distribution of the FGCC-T5 tools were analyzed using EPMA (Figure 1).

Figure 1(a) shows the backscattered electron image of the FGCC-T5 surface. The surface of the tool is formed from two layers: a grey gradient layer (approximately 10 μm thick) and a bright-white substrate layer. During the nitriding sintering process, titanium diffuses to the surface and forms (Ti, W) (C, N) because titanium and nitrogen have a high affinity for each other. At the same time, the space left due to titanium diffusion is filled by tungsten and cobalt coming from the outer layer. Figure 1(b)–(f) shows the results of the EPMA analysis of the

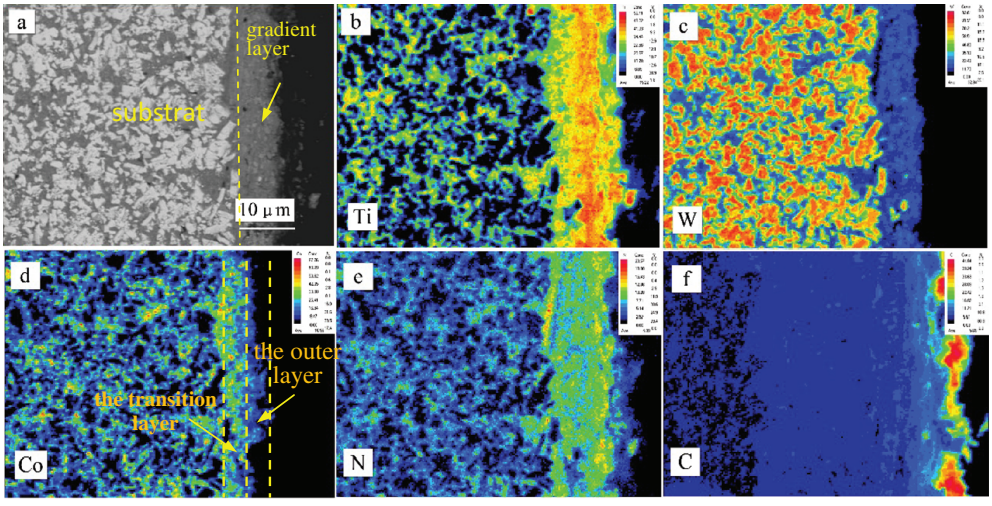

Figure 1: The microstructure of FGCC-T5 cross-sectional metallographic specimens (EPMA, sintering temperature is 1400 °C, holding time is 15 min).

FGCC-T5 samples. It can be seen that the gradient layer is divided into two parts: an outer layer rich in titanium and nitrogen (but deficient in tungsten and cobalt) and an intermediate layer rich in cobalt. As shown in Figure 1(d), the thicknesses of the two layers are essentially equal. Figure 2 shows XRD patterns obtained from the FGCC-T5 tools. It is apparent that the main diffraction peak from the FGCC-T5 surface is due to TiCN. Some small diffraction peaks due to WC and Co can also be seen to exist concurrently. The diffraction peaks measured mainly correspond to the surface components of the tool (as the XRD diffraction depth is about 10 μm). Combining the EPMA results, an outer layer rich in Ti and N is verified. They also show that the TiCN was formed by the nitridation of TiC. An outer layer rich in TiCN will improve the wear resistance of the tools. In addition, the intermediate layer which is rich in cobalt will improve the toughness of the tools and help prevent cracks extending to the substrate.

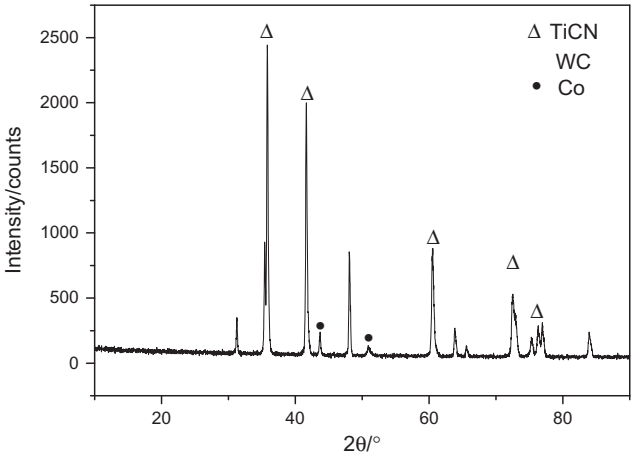

Figure 2: XRD patterns of the gradient layer.

Gradient component distribution model

Based on the EPMA results, a simplified structural model for the component distribution function of the FGCC-T5 was established (Figure 3). In order to facilitate our calculations, the gradient layer was divided into multilayers. The layers with the lowest and highest volume fractions of cobalt are referred to as the Co-poor and Co-rich layers, respectively. Transition layer 1 occurs between the Co-poor and Co-rich layers – transition layer 2 occurs between the Co-rich layer and substrate. The position of Co-rich layer ranges from the Co-poor layer to the substrate according to the thickness ratio between transition layer 1 and transition layer 2. From the surface to the substrate, the FGCC-T5 component distribution is characterized by a gradual decrease in TiCN, a gradual increase in WC, and a parabolic trend (opening downwards) in Co.

In order to better describe the volume fraction of each component, a three-component gradient distribution function was proposed based on a power-law function. In the function, the pores and sintering additives are not taken into account because they have relatively small proportions. The volume fractions of Co, WC and TiCN along the surface-to-substrate direction are given, respectively, by:

$$V_{\mathrm{Co}} = f_1(\xi) = \begin{cases} \left(f_r^{\mathrm{Co}} - f_p^{\mathrm{Co}}\right)\left(\frac{\xi}{k}\right)^{n_1} + f_p^{\mathrm{Co}}, (0 \le \xi \le k) \\ \left(f_r^{\mathrm{Co}} - f_s^{\mathrm{Co}}\right)\left(\frac{1-\xi}{1-k}\right)^{n_1} + f_s^{\mathrm{Co}}, (k \le \xi \le 1) \end{cases} \quad (1)$$

$$V_{\mathrm{WC}} = f_2(\xi) = \begin{cases} \left(f_r^{WC} - f_p^{WC}\right)\left(\frac{\xi}{k}\right)^{n_2} + f_p^{\mathrm{WC}}, (0 \le \xi \le k) \\ \left(f_s^{WC} - f_r^{WC}\right)\left(\frac{\xi-k}{1-k}\right)^{n_2} + f_r^{\mathrm{WC}}, (k \le \xi \le 1) \end{cases} \quad (2)$$

$$V_{\mathrm{TiCN}} = f_3(\xi) = 1 - V_{\mathrm{Co}} - V_{\mathrm{WC}} \quad (3)$$

In these expressions, ξ (or k) denotes the ratio between the distance from an arbitrary position (or to the Co-rich

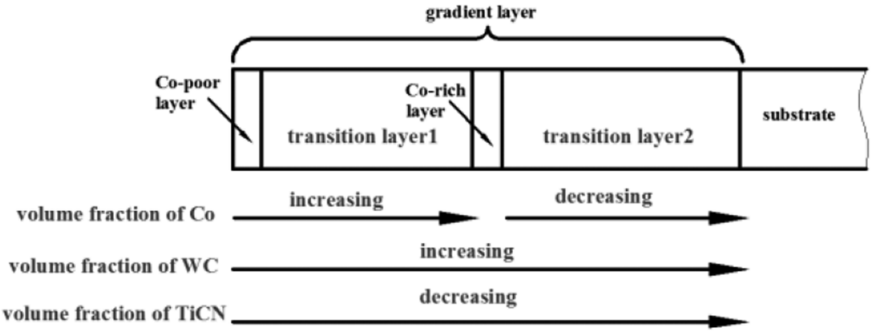

Figure 3: Model of three-component distribution.

layer) to the surface and the total thickness of the gradient layer. The quantities f_p, f_r, and f_s are the volume fractions of each component in the Co-poor layer, Co-rich layer, and substrate, respectively. Finally, n_1 and n_2 are distribution indices.

The volume fraction of a component varies with the sintering parameters employed, which can be described using the different distribution indices. The volume fraction of Co changes from the surface to substrate according to the different distribution indices, as shown in Figure 4. It was found that the distribution function used to describe the composition could properly describe the experimental results.

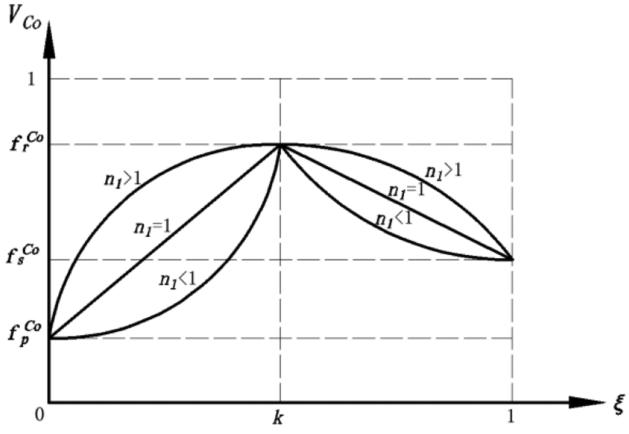

Figure 4: Volume fraction of Co with different distribution indices.

Establishment and validation of the FEM

Finite element modeling

The residual stress of the FGCC-T5 as it cooled from the sintering temperature to room temperature was analyzed using finite element analysis software (ANSYS). The value of the stress and its distribution within the gradient layer were studied. A cylindrical cutter model was used for finite element analysis (Figure 5) and so the origin of the coordinates was chosen to be at the geometrical center of the cylindrical tool section. Directions X and Z are taken to be along the radial and axial directions, respectively. The gradient distribution of each component was calculated using the three-component function. The substrate and gradient layer thicknesses were assigned to d_1 and d_2 in the FEM, respectively. The thickness of the gradient layer of the FGCC-T5 was too small (relative to

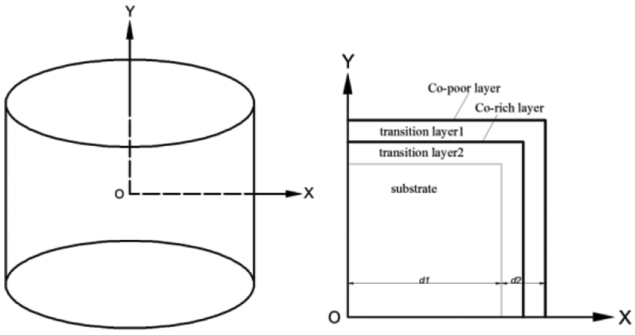

Figure 5: Model of finite element analysis.

the thickness of the substrate), so that only part of the substrate was studied in the calculation model.

The analysis of the residual stress of the FGCC-T5 was simplified using the two-dimensional axial symmetry of the problem in view of the cylindrical symmetry of the cutter. A four-node thermal-stress coupling element was used in the FEM. Boolean algebra was used to handle the gradient layer to ideally bond the multilayers, and these were combined with the substrate of the tool. Parts of the gradient layer where a drastic change in stress occurred were meshed more densely in order to increase accuracy.

The overall temperature field in the model was assumed to change consistently, and the nitriding–sintering and room temperatures were set to $T_1 = 1400\,°C$ and $T_2 = 20\,°C$ in the first instance, respectively. Studies by Bouchafa et al. [22, 23] reported that the effects of a temperature-dependent elastic modulus and thermal expansion coefficient on residual stress are small. Thus, such effects were not taken into account in the present work.

According to our EPMA results, the ratio of the thicknesses of transition layer 1 to transition layer 2 was approximately 1:1, indicating that $k = 0.5$ in eqs (1) and (2). The volume fractions of Co and WC in the Co-poor layer were 5% and 7%, respectively, and those in the Co-rich layer were 35% and 12%, respectively. We set $n_1 = n_2 = 1$ to give linear relationships between the volume fractions and the distance from the surface to an arbitrary position in the first analysis. Residual stress nephograms of the FGCC-T5 are shown in Figure 6.

The distance-dependent residual stress distributions corresponding to different sintering temperatures are shown in Figures 7 and 8. It can be seen from Figure 7 that the highest residual compressive stress is located in the Co-poor layer. Then, this gradually changes to residual tensile stress which peaks in the Co-rich layer. Afterwards, the residual tensile stress gradually falls and finally approaches zero in the substrate. The

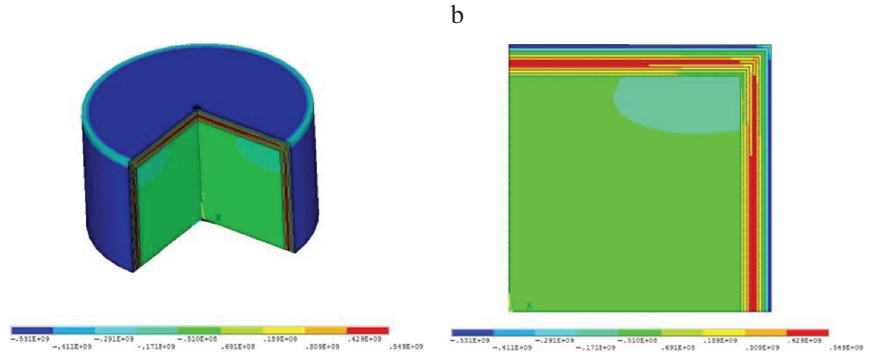

Figure 6: The residual stress nephograms of FGCC-T5 (a-sectional view, b- cross-sectional view).

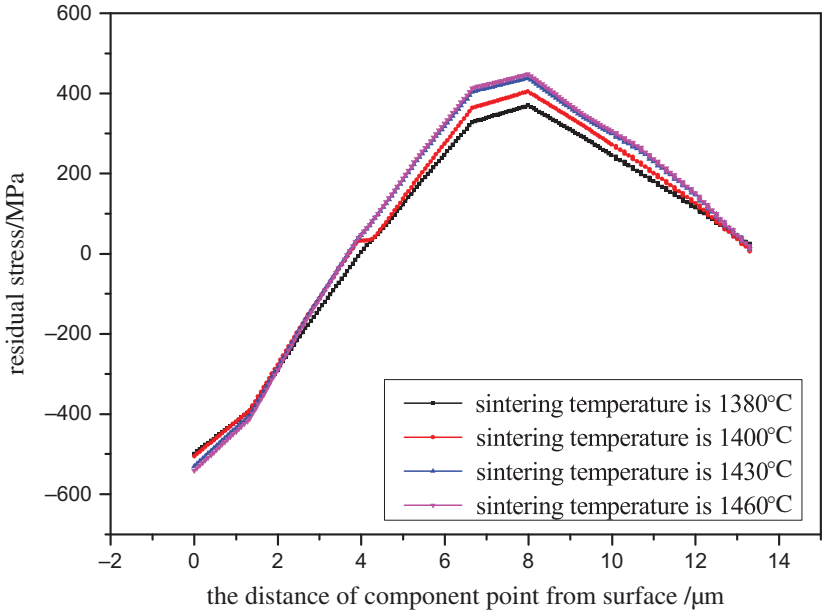

Figure 7: The effect of sintering temperature on residual stress in gradient direction.

maximum residual compressive and tensile stresses in the gradient layer simultaneously increase with increasing sintering temperature. The change in the compressive stress in the Co-poor layer is shown in Figure 8. The compressive stress rapidly increases at first and then changes more slowly with increasing distance from the knifepoint. It can be seen that the lowest compressive stress occurs at the knifepoint due to stress concentration. This thereby became the weakest area of the tool during the cutting process. The compressive stress of the knifepoint increased only slightly with an increase in sintering temperature. At the same time, the location of the region of maximum compressive stress occurred further from the knifepoint in a smaller range.

Feasibility of the finite element method

The residual stress in the FGCC-T5 surface was detected using XRD, which is based on Bragg's law [24]. When X-rays of wavelength λ are irradiated onto a sample, the relationship between the spacing of the crystal planes and inclination angle can be obtained [25]. The residual stress can be calculated using Bruker Leptos software. Figure 9 shows a comparison of the experimental and simulated values of the maximum residual compressive stress. It can be seen that the experimental compressive stress increases from 498 to 581 MPa as the fabrication temperature increases from 1380 to 1460 °C. From 1380 to 1400 °C, the simulated values are

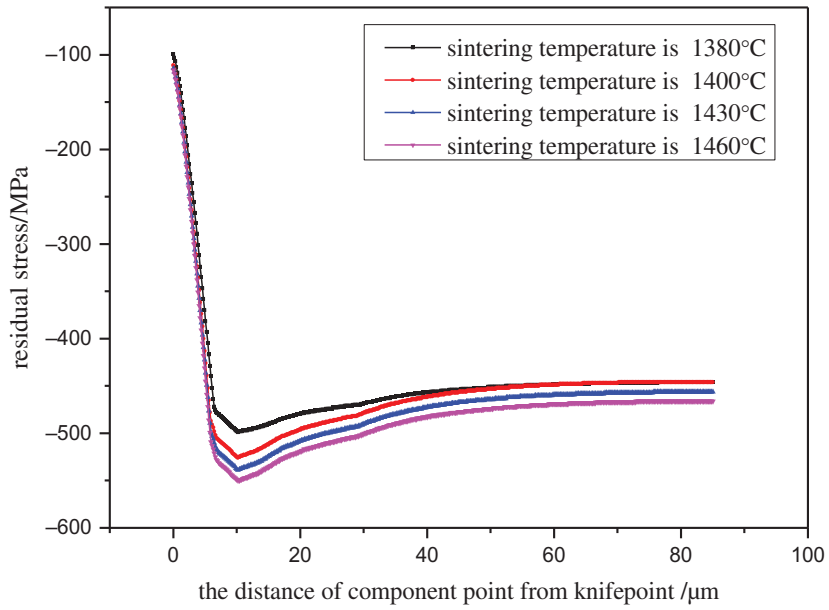

Figure 8: The effect of sintering temperature on residual surface stress.

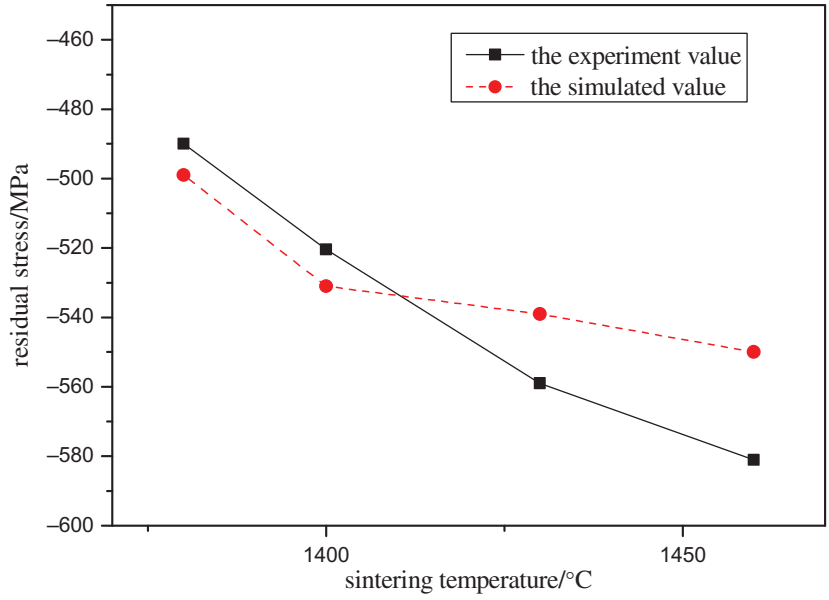

Figure 9: The maximum compression stress of FGCC-T5 by different sintering temperatures.

essentially consistent with the detected values – small differences (3–6 %) are observed, however, over the range 1400–1460 °C. These differences can be attributed to the intensified nitridation that occurs at the higher fabrication temperatures, which leads to greater Co enrichment in the Co-rich layer and more TiCN appearing in the Co-poor layer.

Results and discussion

Effect of gradient distribution index

The beneficial effect of residual stress on cutting performance can be greatly improved by altering the gradient

distribution by controlling the parameters involved in the sintering process. The effect of changing the gradient distribution indices on the residual stress should therefore be explored. As shown in Figure 4, when the distribution index is 1, the component volume fraction changes linearly according to the factor ξ. When the distribution index is smaller (or bigger) than 1, the component volume fraction changes more quickly the closer one is to the Co-rich layer (or Co-poor layer). The effects of varying indices n_1 and n_2 on the residual stress of samples sintered at 1400 °C are shown in Figure 10. It can be seen that for a fixed n_2 (or n_1) and increasing n_1 (or n_2), the maximum residual compressive stress of the gradient layer decreases (or increases). On the other hand, the maximum residual tensile stress increases (or decreases). When n_1 = 0.5 and n_2 = 2.5, the maximum residual compressive stress of the FGCC-T5 was 612 MPa, and the maximum residual tensile stress was 527 MPa. Research by Nomura [3] has shown that when the surface residual compressive stress of a tool reaches 500 MPa, one can be assured that no damage will occur to the tool even in the severest of cutting conditions. Our work indicates that smaller n_1 and bigger n_2 values contribute to the formation of higher residual compressive stress at the surface of the FGCC-T5, and this will thereby improve the tool's cutting performance.

Effect of geometric shape

The knifepoint is directly in contact with the work-piece during the cutting process. Any crack that is initiated in a weak area of the knifepoint will subsequently propagate to the substrate. The analysis above has shown that a right-angled knifepoint provides an asymmetrical residual stress on the surface of the FGCC-T5. Also, the strength of the knifepoint will be reduced if the compressive stress decreases. Figure 11 shows the distribution of

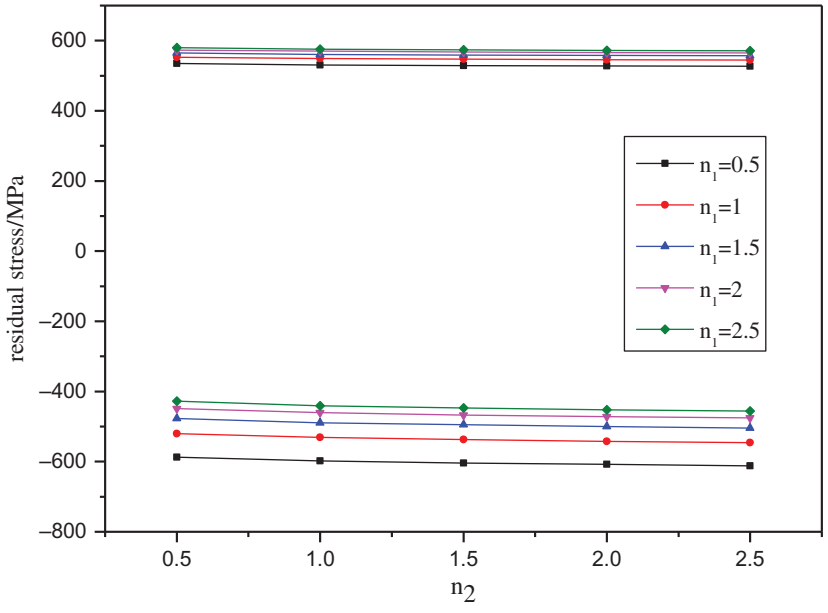

Figure 10: The effect of different gradient distribution indices on residual stress.

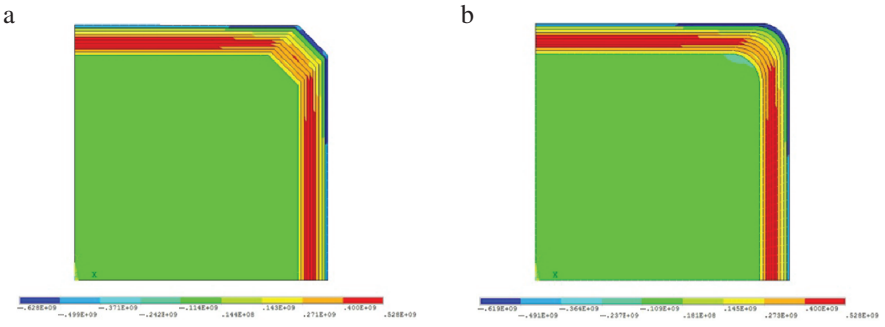

Figure 11: Residual stress distribution of different geometric shape (a) chamfered, (b) rounded-edge.

residual stress corresponding to chamfered and rounded-edge knifepoints. Among the three different types of knifepoint (Figures 6(b) and 11), the residual stress of a rounded-edge knifepoint is the most homogeneous.

The effect of having rounded cutting edges of different radii was also studied (Figure 12). With an increase in radius, the maximum residual surface compressive stress of the tool is reduced while the compressive stress at the knifepoint shows a parabolic trend (opening upwards) and the parabola's peak occurs at a radius of 20 μm. The maximum residual surface compressive stress of the tool and residual compressive stress at the knifepoint changed modestly as the radius of the rounded cutting edge changed. Both values of compressive stress were close to each other when the radius reached 300 μm. Hence, weaknesses in the knifepoint can be avoided by using a knifepoint with a rounded design.

Effect of substrate thickness

The residual stress of the FGCC-T5 in the gradient direction after cooling from a fabricating temperature of 1400 °C to room temperature is shown in Figure 13 for varying substrate thicknesses from 50 to 150 μm. The thickness of the gradient layer and radius of the rounded cutting edge were set 10 and 20 μm, respectively. As the thickness of the substrate increases, the maximum residual compressive stress of the gradient layer decreases. At the same time, the residual tensile stress in the Co-rich layer increases. The residual stress at the knifepoint decreases with increasing substrate thickness, but the differences between the values of the stress for the various thicknesses are small. As residual compressive stress plays an important role in strengthening the tool, the thickness of substrate should be appropriately reduced on the promise of better performance.

Effect of the thickness of the gradient layer

The gradient layer is in direct contact with the work-piece at the surface of the tool. Therefore, it is necessary to study the effect of the thickness of the gradient layer on the residual stress. Figure 14 shows the residual stress of the FGCC-T5 in the gradient direction as the thickness of the gradient layer is changed from 50 to 150 μm. The thickness of the substrate and radius of the rounded cutting edge were set to 75 and 20 μm, respectively. As can be seen from Figure 14(a), as the gradient layer thickness increases, the maximum residual compressive stress of the gradient layer increases from 531 to 712 MPa. However, the compressive stress at the knifepoint (which had a maximum value of 557 MPa when the thickness of the gradient layer was 10 μm), first increased and then decreased. The effect of different gradient layer

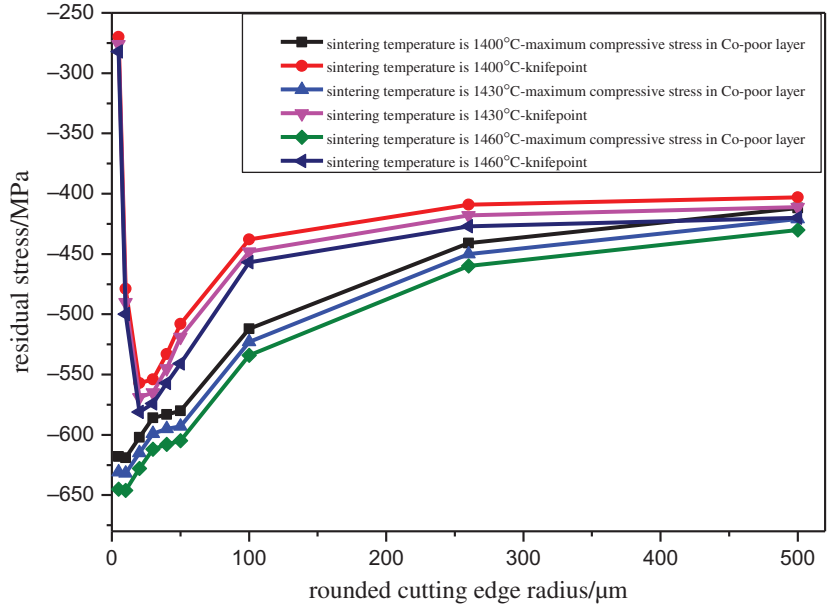

Figure 12: The effect of different rounded cutting edge radius on residual stress.

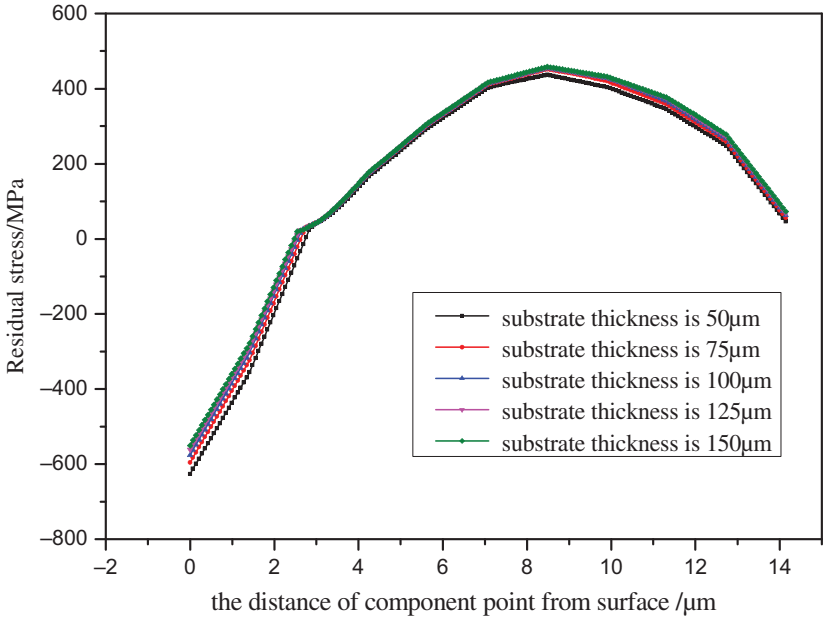

Figure 13: The effect of substrate thickness on residual stress in gradient direction.

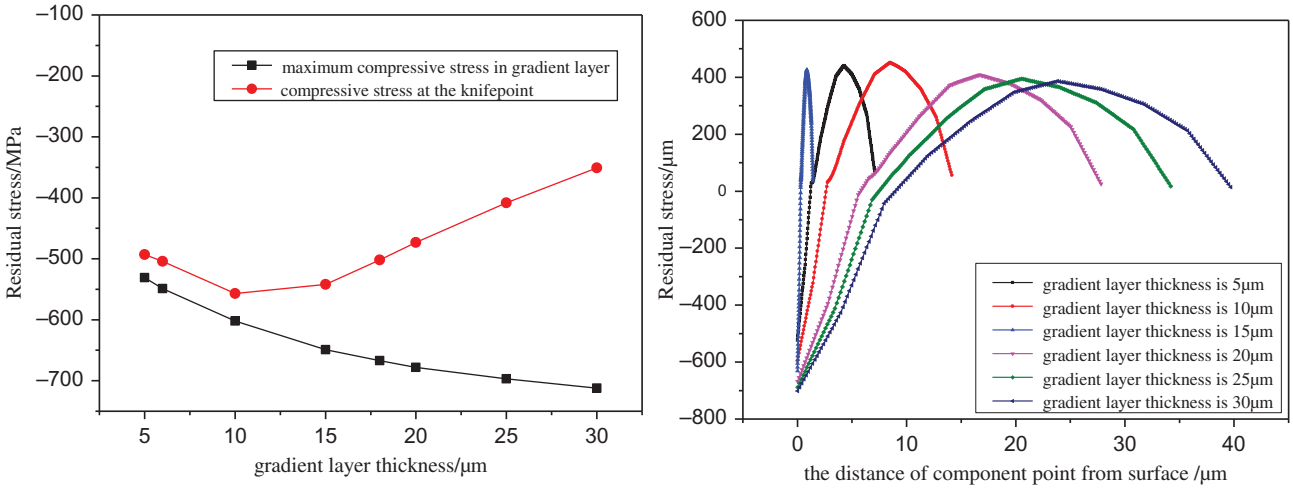

Figure 14: The effect of gradient layer thickness on residual stress (a) compressive stress, (b) residual stress in the gradient direction.

thicknesses on the residual stress in the gradient direction is shown in Figure 14(b). As the gradient layer thickness increases, the distribution of the residual stress in the gradient direction changes little. On the other hand, the region of residual tensile stress increases. Lengauer et al. [26] found that a gradient tool with a 7 μm-thick grade zone produced the best performance in their turning tests. In our work, the compressive stress at the knifepoint exceeded 500 MPa when the gradient layer thickness was between 6 and 18 μm. According to Nomura's criterion [3], therefore, in order to improve the tool's resistance to breakage during the cutting process, the gradient layer thickness should be controlled to be in the range between 6 and 18 μm.

Effect of position of the Co-rich layer

Residual stress is caused by the change in thermal expansion coefficient in the gradient direction. Here, the

thermal expansion coefficient is mainly affected by the position of the Co-rich layer. The Co-rich layer lies between the Co-poor layer and substrate and its position varies by changing the thickness ratio of transition layers 1 and 2.

When the thickness ratio of transition layers 1 and 2 increases from 1:7 to 7:1, the maximum residual compressive stress decreases, and the maximum tensile stress in the Co-rich layer increases (Figure 15). For smaller thickness ratios, the Co-rich layer is closer to the surface of the FGCC-T5, and so the compressive stress in the Co-poor layer is bigger (because the change in the components occurring between the Co-rich and Co-poor layers is more rapid). Therefore, it is important to control the position of the Co-rich layer so that it is close to the tool's surface and to reduce the layer thickness ratio, provided this does not affect the integrity of the tool's surface gradient layer.

Conclusions

In this work, EPMA was used to examine the gradient distribution structure of FGCC-T5 (possessing a cobalt-poor and TiCN-rich layer at its surface and a Co-rich layer as the intermediate layer). Based on the EPMA results, a three-component distribution function for the FGCC-T5 was proposed and the residual stress of the gradient layer formed in the fabrication process analyzed using a finite element method. The feasibility of using FEM to analyze residual stress was verified by comparing the results of the simulations with the experimental results.

The FEM simulations showed that compressive stress is formed in the Co-poor layer and tensile stress is formed in the Co-rich layer. As the sintering temperature was increased, the compressive stress in the surface of the FGCC-T5 also increased. The residual compressive stress in the Co-poor layer was at a maximum when the gradient distribution corresponded to index values of $n_1 = 0.5$ and $n_2 = 2.5$.

A rounded cutting-edge result in compressive stresses that are more symmetrical than those found with right-angled and chamfered edges. When the radius of the rounded cutting-edge was 300 μm, there was no stress concentration at the knifepoint.

As the substrate thickness was increased, the maximum compressive stress in the Co-poor layer decreased and the maximum tensile stress in the Co-rich layer increased. When the location of the Co-rich layer was moved from the surface to the substrate, the compressive stresses of the gradient layer and knifepoint decreased simultaneously. Increasing the thickness of the gradient layer caused the residual compressive stress at the knifepoint to first increase and then decrease. Gradient layers

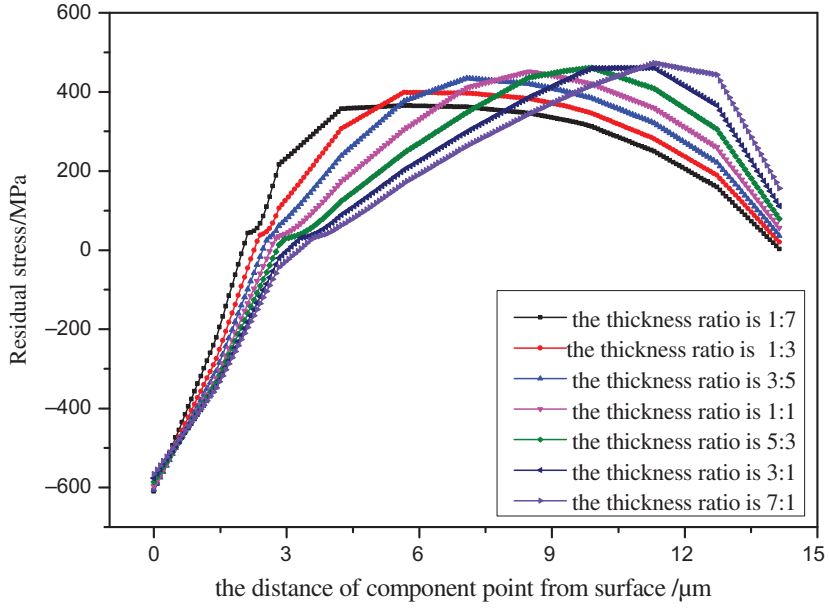

Figure 15: The effect of the Co-rich layer position on residual stress.

with thicknesses between 6 and 18 μm are able to produce enough compressive stress to provide good cutting performance.

Funding: This work was financially supported by National Natural Science Foundation of China (Grant no. 51305134), Scientific Research Fund of Hunan Provincial Education Department (Grant no. 14B057) and Hunan Provincial Innovation Foundation for Postgraduate (Grant no. CX2015B479).

References

1. Weinert K, Inasaki I, Sutherland JW and Wakabayashi T, CIRP. Ann. Manuf. Techn., 2004;53:511–537.
2. Jha DK, Kant T and Singh RK, Compos. Struct., 2013;96:833–849.
3. Nomura T, Moriguchi H, Tsuda K, Isobe K, Ikegaya A and Moriyama, Int. J. Refract. Met. Hard. Mater., 1999;17:397–404.
4. Suresh S and Mortensen A, Fundamentals of functionally graded materials. The Institut of Materials, London, (1998).
5. Fan P, Fang ZZ and Guo J, Int. J. Refract. Met. Hard. Mater., 2013;36:2–9.
6. Demirskyi D, Ragulya A and Agrawal D, Ceram. Int., 2011;37: 505–512.
7. Breval E, Cheng JP, Agrawal DK, Gigi P, Dennis M and Roy R, Mater. Sci. Eng. A., 2005;391:285–295.
8. Lin W, Bai XD, Ling YH, Jiang ZH and Xie ZP, Mater. Sci. Forum, 2003;423:55–58.
9. Tang S, Liu D, Li P, Chen Y and Xiao X, Int. J. Refract. Met. Hard. Mater., 2015;48:217–221.
10. Tanigawa Y, Akai T, Kawamura R and Oka N, J. Therm. Stresses, 1996;19:77–102.
11. Bermejo R, Pascual J, Lube T and Danzer R, J. Eur. Ceram. Soc., 2008;28:1575–1583.
12. Bermejo R, Torres Y, Sanchez-Herencia AJ, Baudin C, Anglada M and Llanes L, Acta Mater 2006;54:4745–4757.
13. Williamson RL, Rabin BH and Drake JT, J Appl Phys 1993;74: 1310–1320.
14. Drake JT, Williamson RL and Rabin BH, J Appl Phys 1993;74: 1321–1326.
15. Huang Z, He Y, Cai H, Xiao Y and Huang B, T. Nonferr. Metal. Soc., 2008;18:660–664.
16. Xu C, Xiao G, Zhang Y and Fang B, Ceram Int 2014;40: 10971–10983.
17. Ai X, Zhao J, Huang C and Zhang J, Mater. Sci. Eng. A 1998; 248:125–131.
18. Xu C, Wu G, Zhang Y, Yi M, Xiao G and Fang B, Chin. J. Mech. Eng-En., 2014;50:94–101.
19. Xu C, Wu G, Xiao G and Fang B, Int. J. Refract. Met. Hard. Mater. 2014;45:125–129.
20. Tang S, Liu D, Li P, Chen Y and Xiao X, High Temp. Mater. Processes. 2015;34:457–460.
21. Tang S, Liu D, Li P, Jiang L, Liu W and Chen Y, Int. J. Refract. Met. Hard. Mater., 2016;58:137–142.
22. Ravichandran KS, Mater. Sci. Eng. A. 1995;201:269–276.
23. Bouchafa A, Benzair A, Tounsi A, Draiche K, Mechab I and Adda Bedia EA, Mater. Des, 2010;31:560–563.
24. Noyan IC and Cohen JB, Residual stress: measurement by diffraction and interpretation. Springer-verlag, New York, 1987.
25. Ligot J, Welzel U, Lamparter P, Vermeulen AC and Mittemeijer EJ, J. Appl. Crystallogr., 2005;38:1–29.
26. Lengauer W and Dreyer K, Int. J. Refract. Met. Hard. Mater., 2006;24:155–161.